Front. Phys. China, 2010, 5(2): 176–182
DOI 10.1007/s11467-010-0020-z
MINI-REVIEW ARTICLE

Ultrafast photoelectric effects and high-sensitive photovoltages in perovskite oxides and heterojunctions

Er-jia GUO (郭尔佳), **Hui-bin LÜ** (吕惠宾)[†], **Kui-juan JIN** (金奎娟), **Guo-zhen YANG** (杨国桢)

Beijing National Laboratory for Condensed Matter Physics, Institute of Physics, Chinese Academy of Sciences, Beijing 100190, China
E-mail: hblu@aphy.iphy.ac.cn

Received March 23, 2010; accepted April 7, 2010

Perovskite oxides and heterojunctions have attracted much attention due to their multifunctional properties of electricity and optics and magnetic as well as the very good chemical and thermal stability. In this brief review, we describe the novel progress of researches in the optical characteristic, including ultrafast photoelectric effects of picosecond order in perovskite oxide single crystals, thin-films and heterojunctions, high-sensitive photovoltages, the enhanced transient lateral photovoltages in perovskite oxide thin-films and heterojunctions, and the high-sensitive ultraviolet (UV) photodetectors based on perovskite oxides. The recent advances present in this paper not only could stimulate theoretical studies on the mechanism but also would open up the possibilities in the developments of optoelectronic devices based on perovskite oxides and heterojunctions.

Keywords perovskite oxides, photoelectric effect, ultraviolet (UV) photodetector

PACS numbers 72.40.+w, 78.66.-w, 85.60.Gz

Contents

1 Introduction 176
2 Novel progress 177
2.1 Ultrafast photoelectric effects 177
2.2 High-sensitive photovoltaic effects in the heterojunctions 178
2.3 High-sensitive UV photodetectors 180
3 Conclusions 181
Acknowledgements 181
References 181

1 Introduction

Perovskite oxides, as one of the leading research topics, have been intensively studied due to their intrinsic properties such as insulating [1], ferroelectric [2, 3], superconducting [4, 5], colossal magnetoresistance (MR) [6, 7], optical properties [8–10] and so on. The fabrication of artificial crystalline materials through layer-by-layer epitaxial growth with full control over the composition and structure at the atomic-scale level has become one of the most exciting areas of research in condensed-matter physics and materials science [11–14]. Heterojunctions and multilayer structures based on the perovskite oxides have emerged as a leading research topic because many novel phenomena and unusual properties have been observed, for instance, unusual positive MR in the heterojunctions of a non-magnetic $SrNb_{0.01}Ti_{0.99}O_3$ (SNTO1) and a negative MR $La_{0.9}Sr_{0.1}MnO_3$ (LSMO1) [15], electrical modulation of MR in multi-p–n heterostructures of $SrTiO_{3-\delta}$/LSMO1/$SrTiO_{3-\delta}$/LSMO1/Si [16], enhancement of second-harmonic generation in $BaTiO_3$/$SrTiO_3$ superlattice [17], polarization enhancement in $BaTiO_3$/$SrTiO_3$/$CaTiO_3$ superlattice [14], and a high-mobility electron gas or even superconductivity in $LaAlO_3$/$SrTiO_3$ heterointerfaces [18, 19]. Optical characteristic, as one of the most important properties in perovskite oxides, has been intensively investigated and made a great progress in recent years. The ultrafast photoelectric effects in perovskite oxide single crystals [20–23], thin films [24] and heterojunctions [25–29], the high-sensitive photovoltaic effects in the heterojunctions [30–33], the transient lateral photovoltage (LPV) induced by Dember effect in p–n heterojunctions [34], and ultraviolet (UV) high-sensitive photodetectors [22, 23, 35, 36] have been reported. In this paper, we describe the recent advances and the future prospects of ultrafast photoelectric effects and high-sensitive photovoltages in the perovskite oxides and heterojunctions.

©Higher Education Press and Springer-Verlag Berlin Heidelberg 2010

2 Novel progress

2.1 Ultrafast photoelectric effects

Figure 1 shows a typical photovoltage pulse when a tilted 15° $SrTiO_3$ (STO) single crystal is irradiated by a 355-nm pulsed laser with 25-ps duration at ambient temperature [20]. The inset of Fig. 1 displays the schematic circuit of the measurement. In order to avoid the influences of external fields and obtain the intrinsic property, we chose the tilted STO single crystal without any applied bias and connected a 0.5-Ω resistance in parallel with STO to measure the open-circuit photovoltages. The photoelectric signals are recorded by a 2.5-GHz bandwidth sampling oscilloscope. The rise time (10%–90%) is about 130 ps, and the full width at half maximum (FWHM) is about 230 ps. The signal polarity of photovoltage pulse is reversed when we illuminate the STO wafer through the reverse face, and no photovoltage signal was observed in untilted STO or when the photon energy of incident light is smaller than the bandgap of STO. The mechanism of the photovoltage in tilted STO single crystals can be understood as following. The STO single crystal absorbs the incident photons and generates the electron–hole pairs as well as a temperature gradient in the irradiation orientation. According to the thermoelectric theory [37], the lateral thermoelectric field can be given by $E(\alpha) = (S_{ab} - S_c)\sin 2\alpha(\mathrm{d}T/\mathrm{d}z)/2$, where S_{ab} and S_c are the Seebeck coefficients along the *ab* plane and *c* axis, α is the vicinal cut angle, and $\mathrm{d}T/\mathrm{d}z$ denotes the temperature gradient in the direction of irradiation. The thermoelectric field leads to the separation of photogenerate carriers in the lateral direction and results the photovoltage we observed.

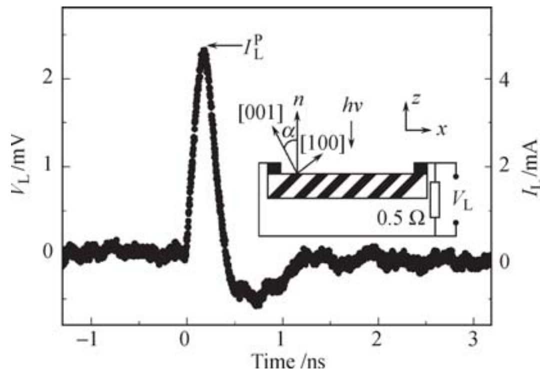

Fig. 1 A typical photovoltage with a 0.5-Ω resistance in parallel with the STO single crystal under an excitation of a 25-ps duration and 355-nm laser pulse. The tilted degree α is 15°. The inset displays the schematic circuit of the measurement. I_L^P denotes the peak value of the transient photocurrent.

Figure 2 shows the peak photovoltage V_L^P and peak photocurrent magnitude I_L^P dependence of the STO tilting angle α [20]. The experimental procedures are the same as shown in Fig. 1. The signal amplitude increases with α until 20° and then decreases. At $\alpha = 45°$, the detected signal, similar to that at $\alpha = 0°$, is almost 0.

Similar to the STO single crystal, we also observed that the response time is 120 ps for $LiNbO_3$ (LNO) single crystal [21], 143 ps for $LiTaO_3$ (LTO) single crystal [22], and 13 ns for $LaAlO_3$ (LAO) single crystal [23].

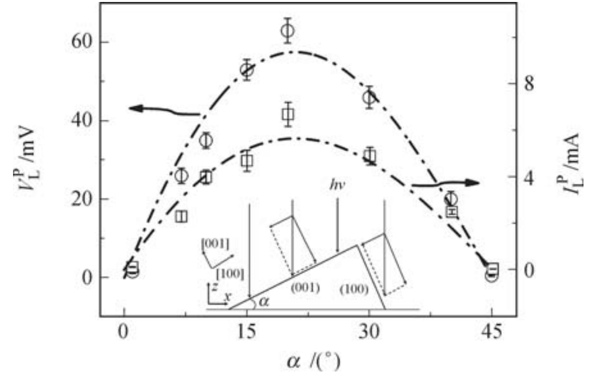

Fig. 2 Peak photovoltage (*open circle*) and peak photocurrent (*open square*) as a function of the tilting angle for the STO single crystals. The dashed lines show the fitting results.

Figure 3 shows a typical open-circuit photovoltage pulse when a $La_{0.67}Ca_{0.33}MnO_3$ (LCMO) film grown on tilted STO substrate is irradiated by a laser pulse of 25-ps duration and 1.064-μm wavelength at ambient temperature [24]. The rise time and the FWHM are as short as 300 and 700 ps, respectively. The photovoltage sensitivity is as large as 0.45 V/mJ, and the photocurrent sensitivity is calculated to 0.25 A/mJ. Similar to the STO single crystal, the mechanism is proposed as the combination of a photoelectron and a Seebeck processes, the Seebeck coefficient we obtained, ∼ 4.04 μV/K, is one order larger than the previous reports.

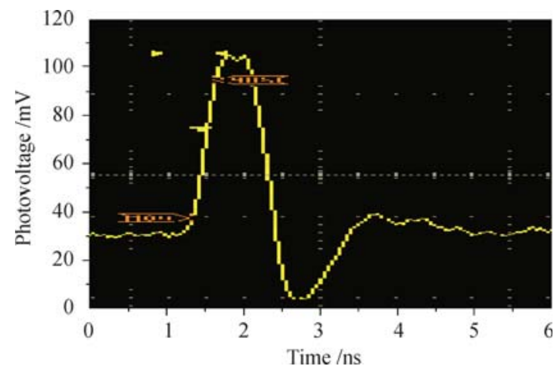

Fig. 3 Variation of the photovoltage with time for LCMO film on tilted 10° STO substrate and a 0.5-Ω resistance is connected in parallel with the LCMO film under an excitation using a 25-ps duration and 1.064-mm laser pulse.

We epitaxial growth $LaAlO_{3-\delta}$, $SrTiO_{3-\delta}$ and $La_{0.7}Sr_{0.3}MnO_3$(LSMO3) thin films on Si substrates by a computer-controlled laser molecular-beam epitaxy (laser-MBE) system and observed the picosecond and nanosecond photoelectric characteristic in the heterojunctions of oxide and Si [26–28]. Figure 4 shows a typical open-circuit photovoltaic pulse of $LaAlO_{3-\delta}$/Si het-

erostructure when the $LaAlO_{3-\delta}$ thin film is irradiated by a 355-nm pulsed laser with 25-ps duration [26]. The inset shows the schematic circuit of the measurement. The waveform was recorded by an oscilloscope with 20 GHz bandwidth. In order to reduce the influences of the measuring system and the capacitance of the p–n heterojunction, a 0.1-Ω resistance is connected in parallel with the $LaAlO_{3-\delta}$/Si heterojunction. The 10%–90% rise time is 86 ps, and the FWHM is 178 ps. The mechanism of the photovoltage in $LaAlO_{3-\delta}$/Si heterojunction can be understood as follows. An n-type $LaAlO_{3-\delta}$ thin film grown onto *p*-type Si substrate could form a p–n heterojunction. The electrons with higher density in n-type $LaAlO_{3-\delta}$ film than those in Si should diffuse into Si, and the holes with higher density in Si than those in $LaAlO_{3-\delta}$ should diffuse into $LaAlO_{3-\delta}$. The diffusion causes a built-in electric field in the space charge region around the interface. With the illumination of light, photogenerated carriers are separated by the built-in field at the interface and caused the photovoltage we measured.

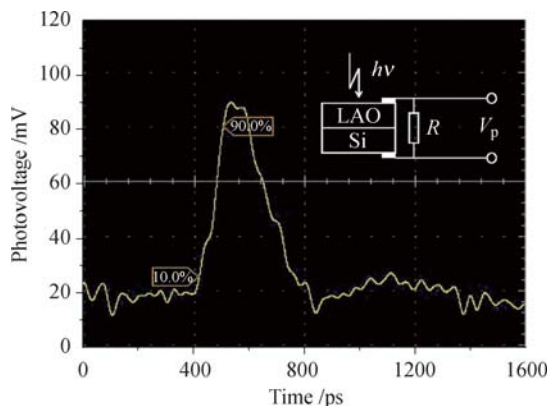

Fig. 4 A typical photovoltaic pulse of LAO/Si p–n junction under the excitation of a 355-nm pulsed laser with 25-ps duration. The inset shows the schematic circuit of the measurement.

Similar to $LaAlO_{3-\delta}$/Si heterostructure, we observed that the response time is 210 ps for LSMO3/Si heterostructure [27], 9 ns for $SrTiO_{3-\delta}$/Si heterostructure [28], and 23 ns for LSMO1/SNTO1 heterostructure [29]. It is noteworthy that all of our experimental results prove that similar to that in the traditional Si semiconductor p–n junction, the photoelectrical process is in a picosecond or nanosecond order in the p–n heterostructures consisting of complex oxides and Si or all oxides.

As mentioned above, the observation of ultrafast photoelectric effects in perovskite oxide single crystals, thin films, and heterojunctions not only proves that the ultrafast photoelectric effect is an intrinsic property of perovskite oxides and heterojunctions but also opens up the application in the development of multifunctional devices.

2.2 High-sensitive photovoltaic effects in the heterojunctions

We observed not only ultrafast photoelectric effects but also high-sensitive photovoltaic effects in the heterojunctions of perovskite oxides. The open-circuit photovoltaic sensitivities are 435 mV/mJ for LSMO3/Si p–n junction [27], 126 mV/mJ for $SrTiO_{3-\delta}$/Si p–n junction [28], and 85.6 V/W for $LaAlO_{3-\delta}$/Si p–n junction [26]. The open-circuit photovoltaic sensitivity can enhance 40 times when a He–Ne laser illuminated the LSMO1/Si p–n junction from the cross-section of the junction than that of from the surface of LSMO1 thin film [31].

Recently, an unusual and rather large LPV has been observed in LSMO1/SNTO1 and LSMO3/Si heterojunctions under the nonuniform irradiation of a pulsed laser [34]. According to the well-established LPV theory of conventional semiconductors, the general understanding of the LPV for semiconductor p–n junctions is that the photogenerated electron–hole pairs balance out a portion of the barrier space charge resulting in a lateral electric field which induces the lateral flow of majority carriers [38]. The LPV effect measured between two random positions on the p side and n side should be reversible because the majority carriers at the p side are holes and those at the n side are electrons. Figure 5(a) and (b) shows the maximum LPV values measured on both sides of the p–n junctions as a function of the laser spot position (x) on the LSMO1 and SNTO1 surfaces in LSMO1/SNTO1 junction, and LSMO3 and Si surfaces in LSMO3/Si junction, respectively [39]. The maximum LPV values were measured on both sides of the p–n junctions; $V_{\mathrm{BA}}^{\mathrm{m}}$ and $V_{\mathrm{ED}}^{\mathrm{m}}$ of the schematic setup for LPV measurements are shown in the insets of Fig. 5(a) and (b). A small area of 0.5 mm in diameter on the *p*-LSMO1 or LSMO3 surface was irradiated by a 308-nm XeCl excimer laser pulse with a pulse width of 20 ns and energy of 0.15 mJ. However, the LPVs are irreversible for both sides of the LSMO1/ SNTO1 p–n junction or LSMO3/Si p–n junction in Fig. 5(a) and (b). This phenomenon challenges the well-established theory of LPV mentioned above for conventional semiconductors. A mechanism based on the difference between the mobility of electrons and holes, that is, the Dember effect [40], was introduced to explain this interesting phenomenon. It should be noticed that the above model of the laser-induced majority carriers dominating LPV effect is only correct when the amount of laser induced carriers is small in the theory of conventional semiconductors. In our experiment, the pulsed laser used in our experiment is a 308-nm XeCl excimer laser beam with an energy density of 0.76 mJ/mm^2 and duration of 20 ns. In this case, the power density of the laser pulse is very high, and the amount of photogenerated carriers should be comparable with or even much larger than that of the majority carriers in the oxide

semiconductor, so that both electrons and holes generated by phonons should play an important role in LPV. In other words, only strong light can cause the Dember-effect-induced LPV in p–n junctions to be observed. As a comparison, Fig. 5(c) shows the Dember-effect-induced LPV in both substrates of SNTO1 and Si measured under the same conditions in Fig. 5(a) and (b). From Fig. 5 (a), (b) and (c), we can see that the enhanced LPV in p–n junctions is 10 times larger than that of LPV in the bulk materials. Actually, the Dember effect has come to a greater prominence recently as a mechanism for generating THz radiation [41].

Figure 6 displays the transient LPV to the laser pulse that depends on the position of the spot in the x axis and undergoes a sign reversal as the laser spot travels from one electrode to the other for the LSMO3/Si junction. The changeover in sign occurs at halfway between the two electrodes (with $x = 0$). The maximum LPV values, $V_{\rm BA}^{\rm m}$, are plotted in Fig. 7 as a function of the laser spot position (x, y) on the LSMO3 surface. In the region between the contacts, $V_{\rm BA}^{\rm m}$ varies quite linearly with x for different y values. The open-circuit position sensitivity, which means the variation of the output photovoltage in V/mJ for a 1 mm displacement of the spot, is about 0.59 (0.39) V/(mJ·mm) for $y = 0(\pm1.5)$ mm, respectively. The response to the irradiation position in the y direction is shown in the inset of Fig. 7. Figure 8 summarizes the spatial distribution of the peak values of LPV in the plane of the junction. The voltage sign reversal is obtained if the spot is moved across the center between the two contacts. The signal is symmetric on the reflection in a plane normal to the y axis at $y = 0$. It is obvious that the large LPV in the p–n junctions is expected to make the candidate for position-sensitive

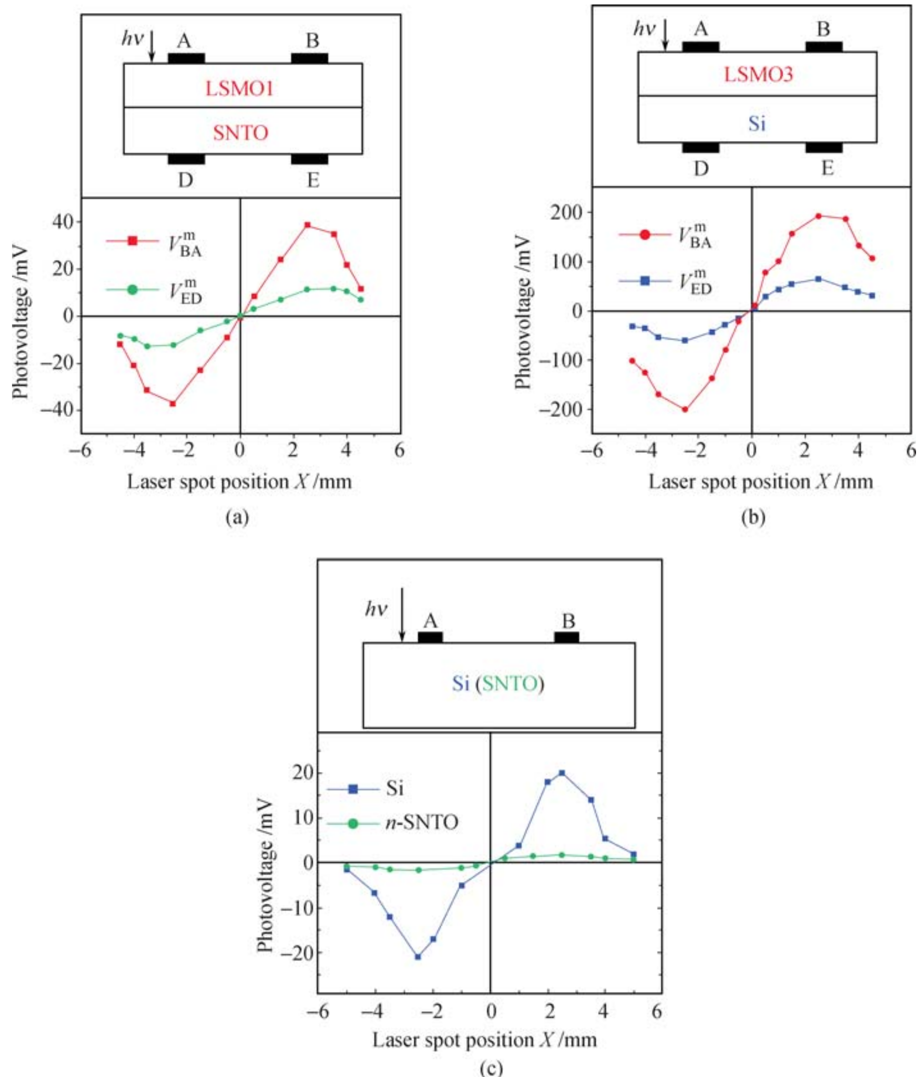

Fig. 5 The peak values of LPV $V_{\rm BA}^{\rm m}$ and $V_{\rm ED}^{\rm m}$ as a function of the position of the laser spot in the x direction in **(a)** the LSMO1/SNTO1 and in **(b)** LSMO3/Si heterostructures, the upper panel displays the schematic setup for the LPV measurement. A (–3 mm), B (3 mm), D (–3 mm), and E (3 mm) denote the electrodes. **(c)** The peak value of LPV, $V_{\rm BA}^{\rm m}$, for n-SNTO (*open triangles*) and Si (*open squares*) substrates.

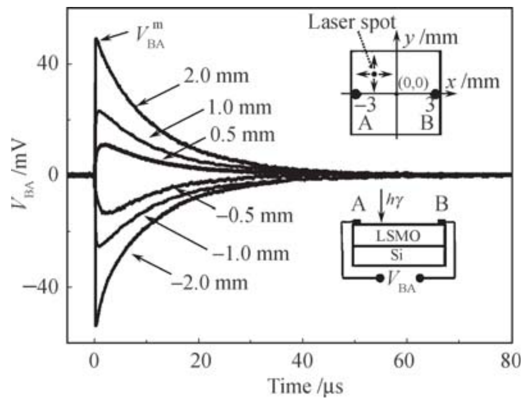

Fig. 6 Transient lateral open-circuit photovoltages after excitation with a 308 nm laser pulse on the LSMO3/Si p–n junction in the x direction at $y = 0$. Numbers in the figure denote the x coordinate values of the laser spot positions. The top inset shows the layout of the sample with contacts A (−3 mm, 0), B (3 mm, 0), and the laser spot (x, y). The bottom one displays the schematic circuit of the V_{BA} measurement.

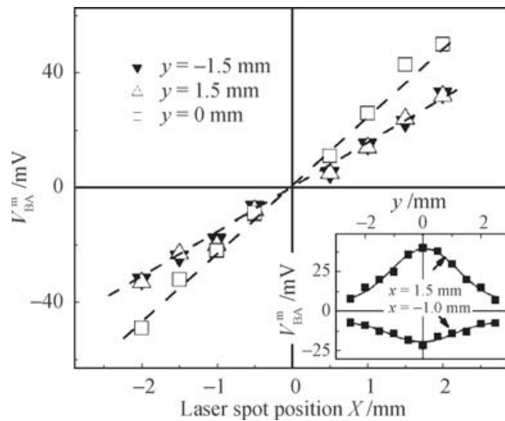

Fig. 7 Dependence of the peak photovoltage $V_{\mathrm{BA}}^{\mathrm{m}}$ on the position of the laser spot in the x direction and y direction (the inset) for the LSMO3/Si p–n junction.

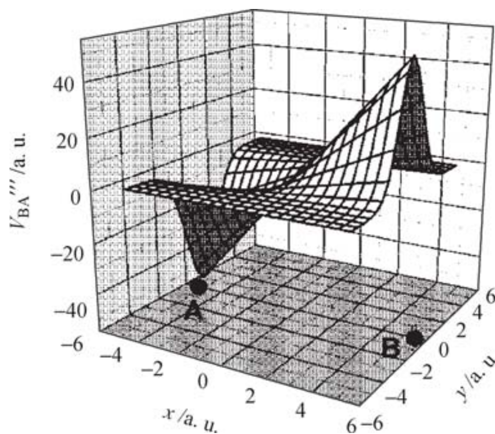

Fig. 8 Three-dimensional plot of LSMO3/Si p–n junction for the $V_{\mathrm{BA}}^{\mathrm{m}}$ as a function of the position of the laser spot.

photodetectors.

2.3 High-sensitive UV photodetectors

UV radiation detectors have drawn a great deal of interest in recent years due to many civil and military requirements. UV est in recent years due to many civil and military requirements. UV detection with high discrimination against visible and infrared light is ideal for detection in the background of infrared and visible radiation. In particular, solar-blind deep-UV detectors can work in a harsh environment of sunlight radiation. Based on the ultrafast photoelectric effects of perovskite oxides, we have successfully fabricated the high-sensitive UV photodetectors using STO [35], LAO [36], LNO [22], and LTO [23] single crystals with interdigitated electrodes.

Figure 9 shows the photocurrent variation with the power density of an STO photodetector with the interdigitated electrodes of 10 μm finger width and 10 μm interspacing at 10 V bias [35]. The inset is the spectral response of the STO photodetector. The cutoff wavelength at 390 nm is very sharp, which corresponds to photon energy of 3.2 eV, agreeing well with the STO bandgap and demonstrating a bandgap excitation process. The UV/visible contrast ratio reaches more than four orders of magnitude. The peak photocurrent responsivity is 213 mA/W located at 330 nm corresponding to the quantum efficiency of 80.2%. The dark current was 50 pA at 10 V bias. The experimental results demonstrate that STO single crystal has potential and wide application in visible-blind UV detection.

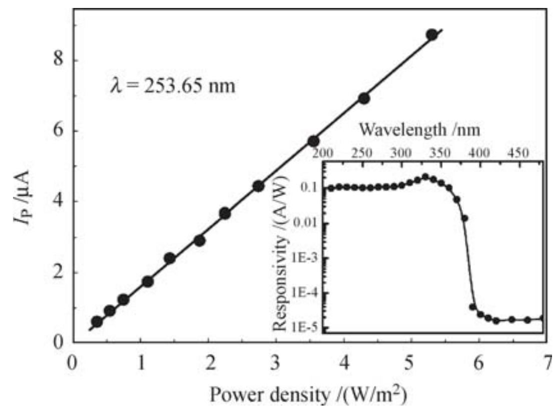

Fig. 9 Photocurrent variation with the power density and the spectral response (inset) of a STO photodetector with 10 μm finger width and 10 μm interspacing at 10 V bias.

Figure 10 shows the spectral response of the LAO photodetector with a finger width of 5 μm and 5-μm interspacing and an effective detection area of 2 × 2 mm at 10-V bias [36]. The inset is the photocurrent variation with the incident light intensity of a D_2 lamp. The sharp cutoff wavelength of the spectrum is located at 220 nm, which corresponds to photon energy of 5.6 eV, agreeing well with the LAO bandgap and demonstrating a bandgap excitation process. The detectors show a high sensitivity to the wavelength less than 210 nm, and the contrast ratio of 200 versus 290 nm is more than two orders of magnitude, indicating that the LAO detector has an intrinsic solar blindness. At a 200-nm wavelength, its photocurrent response is 71.8 mA/W, while its quan-

tum efficiency reaches 44.6%. As shown in Fig. 11 [36], the noise current of LAO detector is only 77 pA under sunlight at midday outdoors, suggesting that the LAO detector can directly detect deep-UV without any filters to block the sunlight.

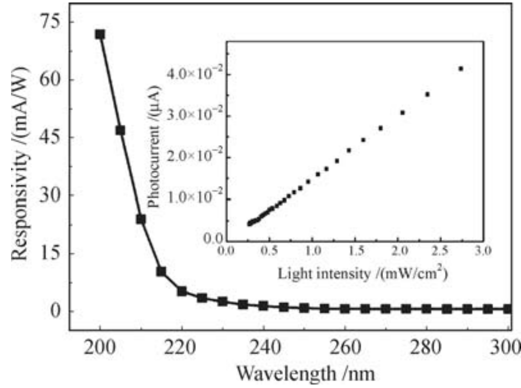

Fig. 10 Spectral response of the LAO photodetector with 5-μm finger width and 5-μm interspacing at 10 V bias. The inset is the photocurrent variation with the incident light intensity of a D_2 lamp.

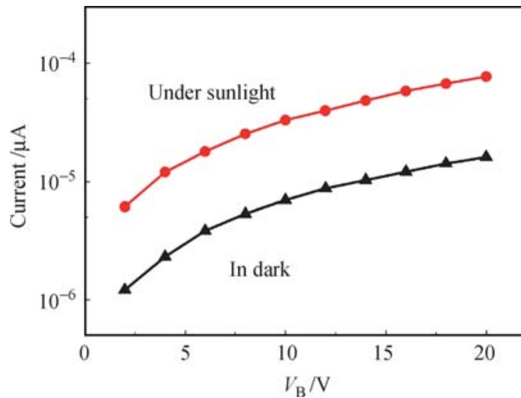

Fig. 11 Bias dependence of the current of the LAO photodetector with 5-μm finger width and 5-μm interspacing measured in the dark and under the irradiation of sunlight at midday.

For LNO photodetector with an interdigitated electrode of 10 μm finger width and 10-μm interspacing, the absorption peak and the absorption edge appear at about 315 and 330 nm, respectively, corresponding to an optical bandgap of ∼3.8 eV. The UV/visible (300 versus 390 nm) contrast ratio is more than two orders of magnitude. The photocurrent response is 17.1 mA/W under the irradiation of 300 nm wavelength UV light at 10-V bias [21].

For an LTO photodetector with interdigitated electrodes of 10-μm finger width and 10-μm interspacing, the response peak appears at about 235 nm and a sharp cutoff at about 270 nm. The noise current is only 61 pA at 20-V bias under the illumination of sunlight at midday outdoors. Similar to the LAO detector, the LTO detector is a solar-blind UV photodetector [22].

The photodetectors mentioned above are based on commercial STO, LAO, LNO, and LTO single crystals and do not need a complicated fabrication technique or process. Their intrinsic characteristics of visible blind and solar blind as well as the excellent high sensitivity demonstrate that the photodetectors based on perovskite oxides with wide bandgap have potential and attractive application in UV detections.

3 Conclusions

In this paper, we described the novel progress in ultrafast photoelectric effects and high-sensitivity photovoltages in perovskite oxides and heterojunctions, such as ultrafast photoelectric effects in perovskite oxide single crystals, thin films, and heterojunctions, high-sensitive photovoltaic effects in the heterojunctions, Dember-effect-induced LPV in perovskite p–n junctions, as well as UV high-sensitive photodetectors. The ultrafast photoelectric effects prove that similar to that in the traditional semiconductor, the photoelectric process is in picosecond order in complex perovskite oxides and heterojunctions, enhancing the confidence to develop the new devices with the perovskite oxide materials. The open-circuit high-sensitive photovoltages as well as Dember-effect-induced LPV have wide applications, such as passive detections, solar cells, and photoelectric control. On the other hand, the high-sensitive photodetectors based on perovskite oxide single crystals with wide bandgap have the potential and attractive applications in UV detection. It is noteworthy that the p–n junctions of oxides and Si combine the multifunctional properties in oxide materials, such as electricity, optics, and magnetism, with Si electronics; such a new structure related to spin ordering, charge carrying, and electron–photon interaction in the system is stimulating a wide study. We believe that the research results present in this paper not only could stimulate theoretical study on the mechanisms but also would open up possibilities in the development of multifunctional devices.

Acknowledgements The authors acknowledge the financial support from the National Natural Science Foundation of China and the National Basic Research Program of China.

References

1. J. H. Barrett, Phys. Rev., 1952, 86(1): 118
2. H. D. Megaw, Nature, 1945, 155: 484
3. H. D. Megaw and D. Helen, Ferroelectricity in Crystals, London: Methuen, 1957
4. J. G. Bednorz and K. A. Muller, Z. Phys. B, 1986, 64(2): 189
5. J. G. Bednorz, M. Takashige, and K. A. Muller, Europhys. Lett., 1987, 3(3): 379
6. S. Jin, T. H. Tiefel, M. McCormack, R. A. Fastnacht, R. Ramesh, and L. H. Chen, Science, 1993, 264: 413
7. A. P. Ramirez, J. Phys.: Condens. Matter, 1997, 9(39): 8171

8. S. Cabuk and A. Mamedov, J. Opt. A: Pure Appl. Opt., 1999, 1: 424
9. S. Hisatake, K. Shibuya, and T. Kobayashi, Appl. Phys. Lett., 2005, 87: 081101
10. T. Zhao, Z. H. Chen, F. Chen, H. B. Lu, G. Z. Yang, and H. S. Cheng, Appl. Phys. Lett., 2000, 77(26): 4338
11. M. Kanai, T. Kawai, and S. Kawai, Appl. Phys. Lett., 1991, 58: 771
12. H. Koinuma and M. Yoshimoto, Appl. Surf. Sci., 1994, 75: 308
13. G. Z. Yang, H. B. Lu, F. Chen, T. Zhao, and Z. H. Chen, Journal of Crystal Growth, 2001, 227: 929
14. H. N. Lee, H. M. Christen, M. F. Chisholm, C. M. Rouleau, and D. H. Lowndes, Nature, 2005, 433: 395
15. H. B. Lu, S.Y. Dai, Z. H. Chen, G. Z. Yang, Y. L. Zhou, M. He, L. F. Liu, H. Z. Guo, Y. Y. Fei, and W. F. Xiang, Appl. Phys. Lett., 2005, 86: 032502
16. K. Zhao, K. J. Jin, H. B. Lu, M. He, Y. H. Huang, G. Z. Yang, and J. D. Zhang, Appl. Phys. Lett., 2008, 93: 252110
17. T. Zhao, Z. H. Chen, F. Chen, W. S. Shi, H. B. Lu, and G. Z. Yang, Phys. Rev. B, 1999, 60: 1697
18. A. Ohtomo and H. Y. Hwang, Nature, 2004, 427(6973): 423
19. E. Dagotto, Science, 2007, 318(5853): 1076
20. K. Zhao, K. J. Jin, Y. H. Huang, S. Q. Zhao, H. B. Lu, M. He, Z. H. Chen, Y. L. Zhou, and G. Z. Yang, Appl. Phys. Lett., 2006, 89: 173507
21. E. J. Guo, J. Xing, K. J. Jin, H. B. Lu, J. Wen, and G. Z. Yang, J. Appl. Phys., 2009, 106(2): 023114
22. E. J. Guo, J. Xing, K. J. Jin, H. B. Lu, J. Wen, and G. Z. Yang, Ultraviolet fast-response photoelectric effects in $LiTaO_3$ single crystal, J. Phys. D: Appl. Phys., 2010, 43(1): 015402
23. X. Wang, J. Xing, K. Zhao, J. Li, Y. H. Huang, K. J. Jin, M. He, H. B. Lu, and G. Z. Yang, Physica B, 2007, 392(1–2): 104
24. K. Zhao, K. J. Jin, Y. H. Huang, H. B. Lu, M. He, Z. H. Chen, Y. L. Zhou, and G. Z. Yang, Physica B, 2006, 373: 72
25. J. R. Sun, C. M. Xiong, B. G. Shen, P. Y. Wang, and Y. X. Weng, Appl. Phys. Lett., 2004, 84(14): 2611
26. J. Wen, K. J. Jin, M. He, H. B. Lu, F. Yang, and G. Z. Yang, Appl. Phys. Lett., 2009, 94: 061118
27. H. B. Lu, K. J. Jin, Y. H. Huang, M. He, K. Zhao, B. L. Cheng, Z. H. Chen, Y. L. Zhou, S. Y. Dai, and G. Z. Yang, Appl. Phys. Lett., 2005, 86: 241915
28. K. Zhao, Y. H. Huang, Q. L. Zhou, K. J. Jin, H. B. Lu, M. He, B. L. Cheng, Y. L. Zhou, Z. H. Chen, and G. Z. Yang, Appl. Phys. Lett., 2005, 86: 221917
29. Y. H. Huang, K. J. Jin, K. Zhao, H. B. Lu, M. He, Z. H. Chen, Y. L. Zhou, G. Z. Yang, and X. L. Ma, Chin. Phys. Lett., 2006, 23(4): 982
30. K. Zhao, K. J. Jin, H. B. Lu, Y. H. Huang, Q. L. Zhou, M. He, Z. H. Chen, Y. L. Zhou, and G. Z. Yang, Appl. Phys. Lett., 2006, 88: 141914
31. J. Xing, K. Zhao, G. Z. Liu M. He, K. J. Jin, and H. B. Lu, J. Phys. D: Appl. Phys., 2007, 40(19): 5892
32. J. Xing, K. J. Jin, H. B. Lu, M. He, G. Z. Liu, J. Qiu, and G. Z. Yang, Appl. Phys. Lett., 2008, 92: 071113
33. H. Liu, K. Zhao, N. Zhou, H. B. Lu, M. He, Y. H. Huang, K. J. Jin, Y. L. Zhou, G. Z. Yang, S. Q. Zhao, A. J. Wang, and W. X. Leng, Appl. Phys. Lett., 2008, 93: 171911
34. K. J. Jin, K. Zhao, H. B. Lu, L. Liao, and G. Z. Yang, Appl. Phys. Lett., 2007, 91: 081906
35. J. Xing, K. Zhao, H. B. Lu, X. Wang, G. Z. Liu, K. J. Jin, M. He, C. C. Wang, and G. Z. Yang, Opt. Lett., 2007, 32(17): 2526
36. J. Xing, E. J. Guo, K. J. Jin, H. B. Lu, J. Wen, and G. Z. Yang, Opt. Lett., 2009, 34(11): 1675
37. H. Lengfellner, G. Kremb, A. Schnellbögl, J. Betz, K. F. Renk, and W. Prettl, Appl. Phys. Lett., 1992, 60(4): 501
38. S. Amari, J. Phys. III France, 1991, 1(10): 1669
39. K. J. Jin, H. B. Lu, K. Zhao, C. Ge, M. He, and G. Z. Yang, Adv. Mater., 2009, 21: 1
40. J. I. Pankove, Optical Processes in Semiconductors, Englewood Cliffs, NJ: Prentice-Hall Inc., 1971
41. R. Kersting, K. Unterrainer, G. Strasser, H. F. Kauffmann, and E. Gornik, Phys. Rev. Lett., 1997, 79: 3038